Available online at www.sciencedirect.com
ScienceDirect
Trans. Nonferrous Met. Soc. China 22(2012) 2041−2048
Transactions of Nonferrous Metals Society of China
www.tnmsc.cn

Cyclic oxidation of Y_2O_3-modified ultrafine-grained Ni_3Al alloy coating at 900 °C

ZHOU Yue-bo, ZHANG Hai-jun

College of Materials Science and Engineering, Heilongjiang Institute of Science and Technology, Harbin 150027, China

Received 20 August 2011; accepted 27 February 2012

Abstract: Ni_3Al coatings with and without Y_2O_3 particles were developed by annealing the electrodeposited Ni−Al composite coatings with and without Y_2O_3 particles at 800 °C for 3 h. The microstructures and cyclic oxidation performances of the produced Ni_3Al coatings were comparatively investigated, with the emphasis on the effect of Y_2O_3. SEM/EDAX and TEM characterizations showed that the dispersion of Y_2O_3 refines the grains. Oxidation at 900 °C for 100 h showed that the addition of Y_2O_3 significantly improved the cyclic oxidation resistance of Ni_3Al coating. The effect of Y_2O_3 on the microstructure and the oxidation of the Ni_3Al coating were discussed in detail.

Key words: electrodeposition; Ni_3Al; cyclic oxidation; reactive element effect

1 Introduction

Ni_3Al coating has been developed using different coating techniques because of its attractive applications in the aerospace and power industries due to the formation of thermodynamically stable Al_2O_3 scale at high temperatures [1,2]. Recently, Ni−Al alloy coatings with good isothermal oxidation resistance due to the formation of alumina scale were developed by the heat-treatment of electrodeposited Ni−Al composite coatings [3−7]. However, the cyclic oxidation resistance of such alloys or coatings is inherently poor, because the scale formed is susceptible to spalling [6−8]. Currently, the formation of poorly adherent alumina scale has been correlated with a decrease in the scale/metal interface strength because of interface segregation of sulfur, a common impurity in metals which can weaken the interfacial bonding [9], and because of the formation of large interface void [10]. It was reported that the grain refining may help an alumina-forming alloy to thermally develop a much adherent alumina scale [1,11,12]. However, the grain coarsening during oxidation may significantly decrease the cyclic oxidation resistance in the long-term. Doping with a small amount of reactive element (RE), such as Y, Ce, La or their oxides, could effectively improve the scale adherence and suppress the spallation in alumina-forming alloys and coatings [13−15] due to the presence of RE or its oxides either in metals or at the scale/metal interface profoundly retarding the formation of the interfacial cavities [10,11] or effectively decreasing the interfacial activity of sulfur [9], which was called the "reactive element effects" (REE). RE or RE oxides are commonly added into alloys or coatings by different techniques [13−15]. Electro-deposition is another technique to co-deposit RE oxide particles in composite coatings by adding RE oxide particles to the plating bath [3,4,6,7]. The current authors [16,17] found that the codeposited Y_2O_3 or CeO_2 particles significantly improved the isothermal oxidation resistance of Ni−Al alloy coatings. LIU and CHEN [4,6,7] found that the pores in micron size and the oxidation temperature affected the cyclic oxidation resistance of the Ni_3Al coatings. At a comparable pore, the codeposited CeO_2 significantly enhanced the cyclic oxidation resistance of Ni_3Al coatings. Y_2O_3 had little effect on the two-phase, γ-Ni+γ'-Ni_3Al, coatings due to different volume fraction of pores, which depended on the Al content in the Ni−Al composite coatings [4]. However, PENG et al [12] found that pores (around 8.6% volume fraction) in submicron size had no deterimental effect on the scale adhesion of the Ni_3Al

Foundation item: Project (11531319) supported by Scientific Research Fund of Heilongjiang Provincial Education Department, China
Corresponding author: ZHOU Yue-bo; Tel: +86-451-88036159: E-mail: zhouyuebo760309@163.com; ybzhou@imr.ac.cn
DOI: 10.1016/S1003-6326(11)61426-X

coating at 900 °C. However, the comparison of cyclic oxidation of the Ni_3Al coatings with and without Y_2O_3 particles at a comparable pores has not been reported, and the effect of Y_2O_3 particles on the cyclic oxidation behaviors of Ni_3Al coatings is unclear. In order to elucidate the effect of base metal on the oxidation behavior of Ni_3Al coatings [3,4], the electrolytic Ni plate was chosen as base metal. The aim of this work is to gain an understanding of the effect of Y_2O_3 on the cyclic oxidation behaviors of Ni_3Al coatings at 900 °C.

2 Experimental

Pure nickel specimens with the dimensions of 15 mm×10 mm×2 mm were cut from a pure electrolytic nickel plate and then were abraded by 800 grit SiC waterproof paper. After being ultrasonically cleaned in acetone, the specimens were electrodeposited a 70−80 μm-thick film of Ni−Al−Y_2O_3 or Ni−Al composite in a nickel sulfate bath. The detailed coating process was provided elsewhere [16−19]. After being ultrasonically cleaned in distilled water, both the composite coatings were annealed in a sealed quartz tube filled with pure Ar atmosphere at 800 °C for 3 h. To remove the oxide scale formed during annealing, a surface zone of ~5 μm thickness was ground from the annealed samples using 1000 grit SiC paper. In order to get Ni_3Al coatings with a comparable Al content and porosity, the energy-dispersive X-ray analysis (EDAX) of the middle of the cross-sectioned composite films after annealing was conducted. The coatings with and without Y_2O_3 particles contained (12.9±0.3)% Al based on the direct measurement of 10 different areas, a content locating in the narrow nonstoichiometric domain of Ni_3Al was chosen for experiment. Theoretically, the produced Ni_3Al coatings would have the porosity of 8.6% (volume fraction). EDAX showed the Y_2O_3 content was 3%−7% (mass fraction) for the Y_2O_3-diepersed Ni_3Al coating.

Cyclic oxidation test at 900 °C in air up to 100 h was performed by automatically lifting samples in the hot zone of a vertical furnace after a 1 h exposure followed by a 10 min cooling to room temperature. Mass changes of the oxidized specimens were measured after fixed time intervals using a balance with 0.01 mg sensitivity. The phase composition and microstructure of the coatings before and after oxidation were investigated using TECNAI−20 type transmission electron microscope (TEM), Camscan MX2600FE type scanning electron microscope with energy dispersive X-ray analysis (SEM/EDAX) and D/Max−2500 pc type X-ray diffractometer (XRD), respectively. Electroless Ni-plating was plated on the surface of the oxidized specimens to prevent the spallation of the scales for observing cross-sections.

3 Results

3.1 Microstructure

Figure 1 shows some parallel TEM bright-field images of Ni−Al−Y_2O_3 composite. Although the distribution of Al and Y_2O_3 microparticles could be observed in some locations (Fig. 1(a)), the particles were not present in most areas. A representative TEM image without Al and Y_2O_3 microparticle is presented in Fig. 1(b). The image reveals that the coating generally contains Ni grains in size of 100−200 nm. The grain size is close to the grain size of electrodeposited Ni−Al composite film without Y_2O_3 microparticle, as reported elsewhere [18]. After 3 h annealing at 800 °C, the Al particles fully reacted with Ni to form γ'-Ni_3Al according to the XRD analysis (Fig. 2) and the image of cross-sections of the coatings before and after annealing treatment (Fig. 3), which caused numerous pores in submicron size due to the volume shrinkage [3−7,16,17]. However, the coatings were still adherent to the Ni base. A similar phenomenon occurred on the Ni−12.9Al composite [17]. Y_2O_3 particles were observed in Ni−Al−Y_2O_3 coatings before and after annealing, as arrowed in Figs. 3(b) and (d). However, the peaks of Y_2O_3 phases in XRD analysis were not detected due to the low concentration.

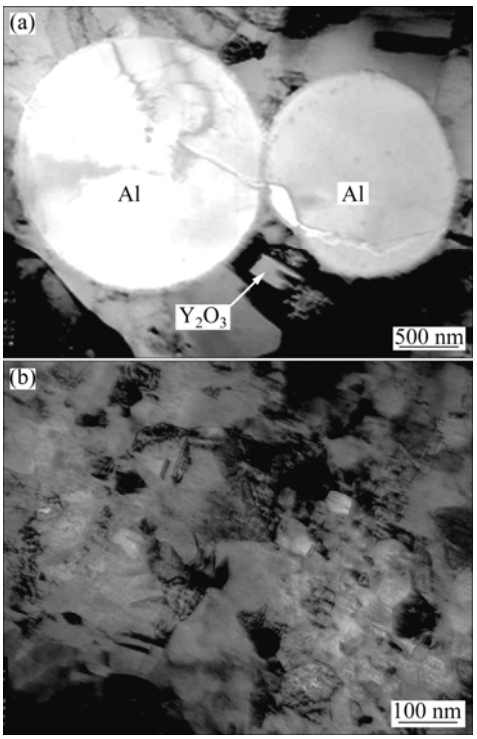

Fig. 1 TEM bright-field images of as-deposited Ni−Al−Y_2O_3 composites in area with (a) and without (b) Y_2O_3 and with Al particles

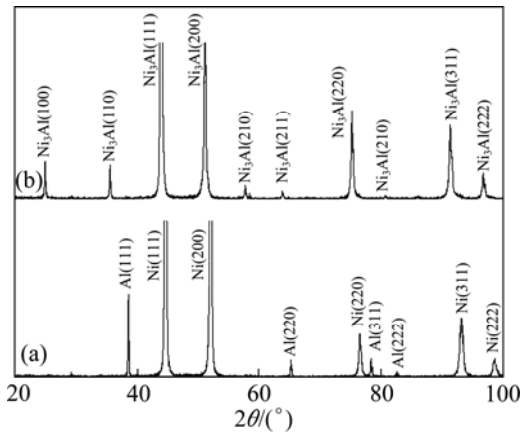

Fig. 2 XRD patterns of as-deposited Ni−Al−Y_2O_3 coating before (a) and after (b) annealing treatment

TEM observations showed that the grain size of the Y_2O_3-free γ'-Ni_3Al coating was generally large than 1 μm [17], while that of the Y_2O_3-dispersed γ'-Ni_3Al coating was ultrafine-grained (~500 nm) (Fig. 4(a)), indicating that the grain growth of the Y_2O_3-dispersed Ni_3Al coating was retarded by the dispersed Y_2O_3. Figures 4(b) and (c) show a bright-field TEM image and the corresponding SAED pattern of the dispersion bright Y_2O_3 particles in the Y_2O_3-dispersed γ'-Ni_3Al coating. It can be seen that near the Y_2O_3 particles, finer grain occurs. Furthermore, the dispersoids of about 50 nm (as arrowed in Fig. 4(b)) are much smaller than the original Y_2O_3 particles used, suggesting the dissolution and re-precipitation of some Y_2O_3 particles during the annealing process.

3.2 Oxidation resistance

Figure 5 illustrates the mass gain vs time curves after cyclic oxidation of γ'-Ni_3Al coating with and without Y_2O_3 in air at 900 °C for 100 h. In the first 40 h, no scale spallation was observed for both coatings. However, the Y_2O_3-dispersed γ'-Ni_3Al coating exhibited lower mass gain than the Y_2O_3-free γ'-Ni_3Al coating. After 40 h, scale spallation and significant mass gain can be observed for the Y_2O_3-free γ'-Ni_3Al coating, suggesting the regrowth of less protective scale on the spallation areas. The spallation was also viewed by naked eyes. After 60 h, the mass loss by spallation became larger than the mass gain by oxidation. In contrast, no significant spallation was observed during the entire thermal cycling of the Y_2O_3-dispersed γ'-Ni_3Al coating.

XRD characterization indicated that the oxides formed on the Y_2O_3-free γ'-Ni_3Al coatings were composed of Al-rich oxides ($NiAl_2O_4$ and Al_2O_3) and NiO, while Al_2O_3 was the main oxide formed on the Y_2O_3-dispersed γ'-Ni_3Al coating, no NiO and $NiAl_2O_4$ spinel peaks were detected. This suggests that the Y_2O_3 significantly suppresses the growth of NiO and $NiAl_2O_4$ during the thermal cycling of the γ'-Ni_3Al coatings. This was also visually confirmed by SEM/EDAX investigation. Figure 6(a) shows the surface morphology of the Y_2O_3-free γ'-Ni_3Al coating after oxidation in air

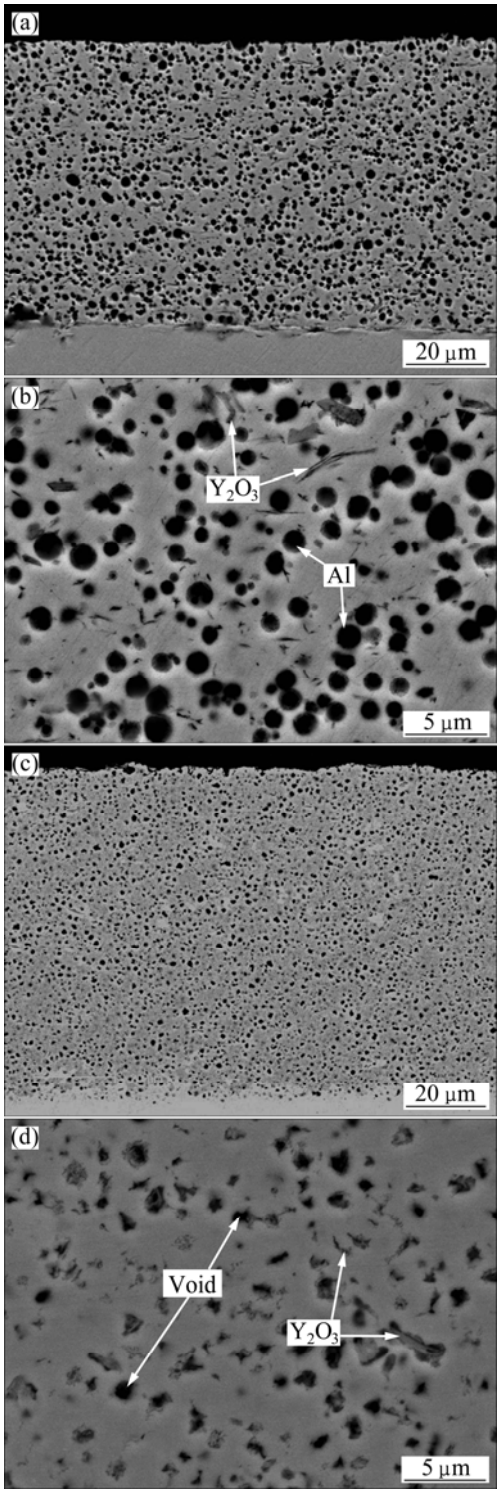

Fig. 3 Cross-sectional backscattered electron (BSE) SEM images of as-deposited (a, b) and as-annealed (c, d) Ni−Al−Y_2O_3 composite

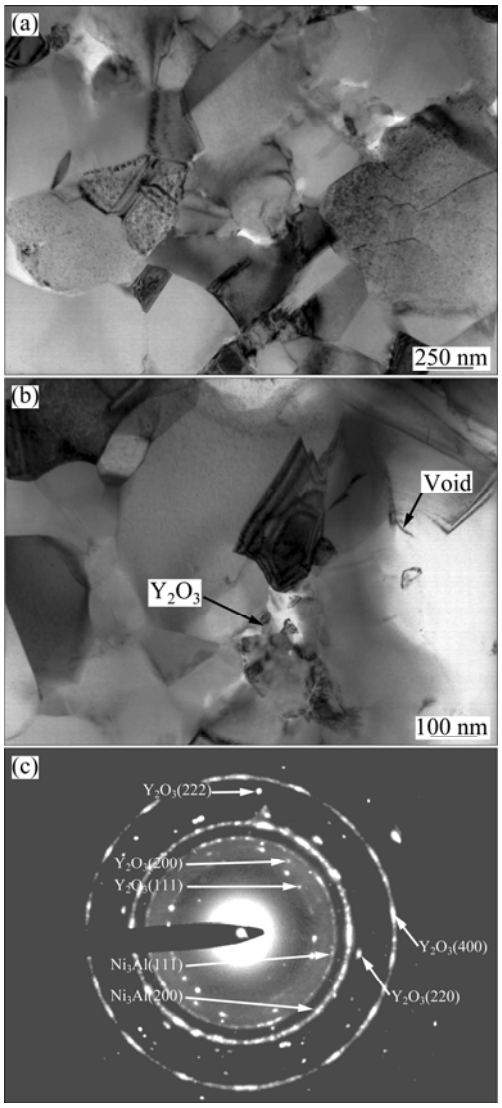

Fig. 4 TEM bright-field images of Y_2O_3-dispersed Ni_3Al coating: (a) A major area without distribution of Y_2O_3 particles; (b) An area with Y_2O_3 particle dispersion; (c) Corresponding SAED pattern

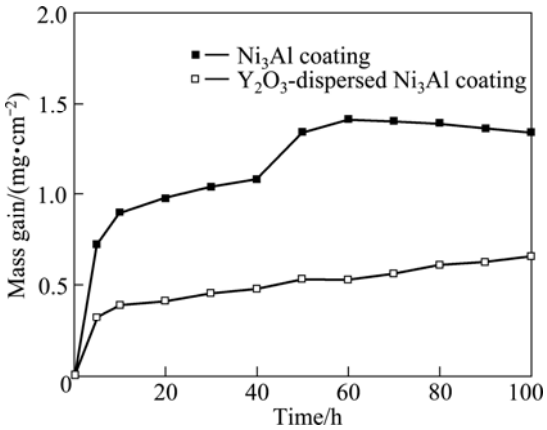

Fig. 5 Cyclic oxidation curves of Ni_3Al samples oxidized in air at 900 °C for 100 h

for 100 h. Heavy spallation occurred. From a magnified image in the inset, large interface cavities were observed. In addition to those formed during the annealing treatment, voids with different size were also observed in oxide scales left on the surface (as arrowed in Fig. 6(a)). A magnified image with spallation area was presented in Fig. 6(b), in which NiO nodule was

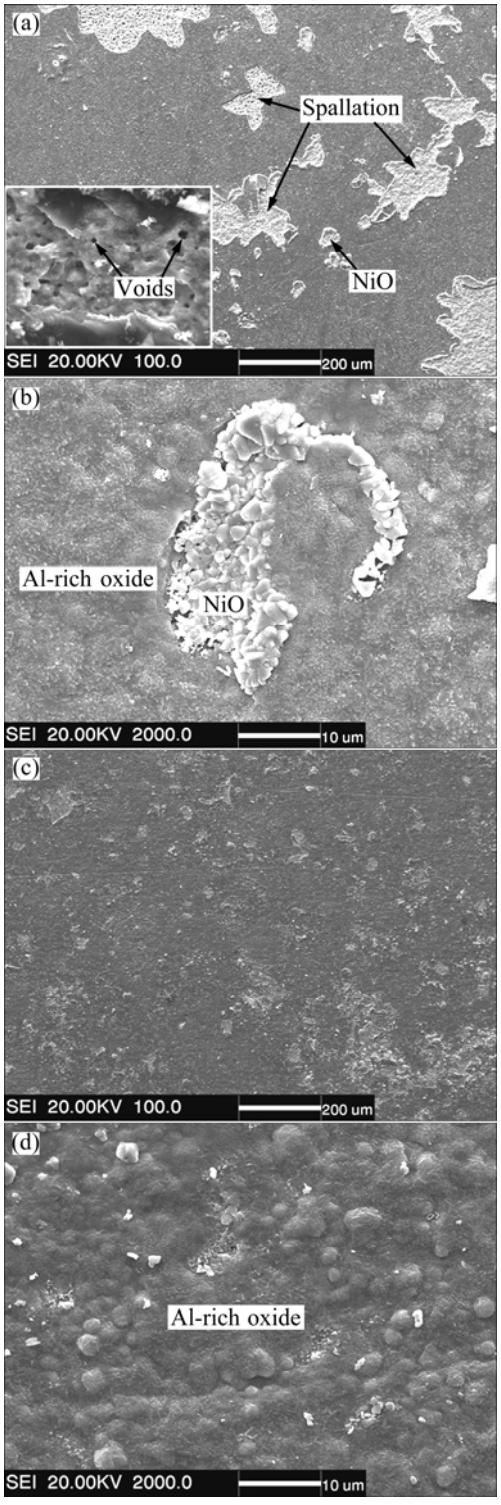

Fig. 6 Surface second electron images of oxide scales formed on pure Ni_3Al (a, b) and Y_2O_3-dispersed Ni_3Al (c, d) coatings after cyclic oxidation in air at 900 °C for 100 h

visible on spallation area and Al_2O_3 (possibly including $NiAl_2O_4$ spinel) appeared on most other areas. In contrast, no spallation was visibed on the Y_2O_3-dispersed γ'-Ni_3Al coating after oxidation in air for 100 h, as shown in Fig. 6(c). A silimar Al-rich oxide scale morphology as the Y_2O_3-free γ'-Ni_3Al coating (Fig. 6(b)) appears, as shown in Fig. 6(d).

The fractured cross-sectional morphology of the Y_2O_3-dispersed Ni_3Al coating after 100 h cyclic oxidation in air at 900 °C is presented in Fig. 7. The thin Al-rich oxide scale had a columnar-grain structure. The scale structure was very silmilar to that formed on the CeO_2-dispersed γ'-Ni_3Al coating at 1050 °C [7]. The scale was dense and no voids were seen at the grain boundaries and the scale/coating interface. It means that if voids can form, they are too fine to be visible in the magnification.

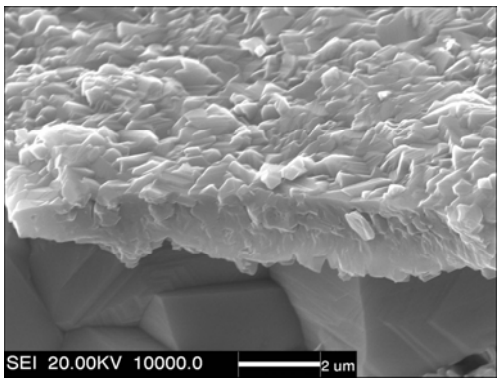

Fig. 7 Fractured cross-sectional image of Y_2O_3-dispersed Ni_3Al coating after cyclic oxidation in air at 900 °C for 100 h

Figure 8(a) shows a scale cross-section passing through one NiO nodule formed on the Y_2O_3-free γ'-Ni_3Al coating. A thin Al-rich scale layer (indicated by arrow) can be clearly seen in the middle of the NiO nodule. This layer is almost parallel to the surface oxide layer around the NiO nodule. This observation strongly suggests that the Al-rich scale layer in the NiO nodule is linked with the alumina layer around the nodule before its formation. From a magnified image given in Fig. 8(b), the inner alumina layer (the "dark" continuous layer close to the metal) and the external less protective $NiAl_2O_4$ spinel (the "grayish" area) are clearly seen on the other areas without NiO nodule. NiO is also locally visible at the spallation-free area. Below the scale some cavities formed, as clearly indicated in Fig. 8(b). The scale structure is very similar to that formed on the electrodeposited Ni−28Al nanocomposite after 126 h cyclic oxidation at 1000 °C [19]. In contrast, during the thermal cycling of the Y_2O_3-dispersed γ'-Ni_3Al coating, no spallation and NiO nodules were observed, as shown in Fig. 8(c). From the corresponding higher

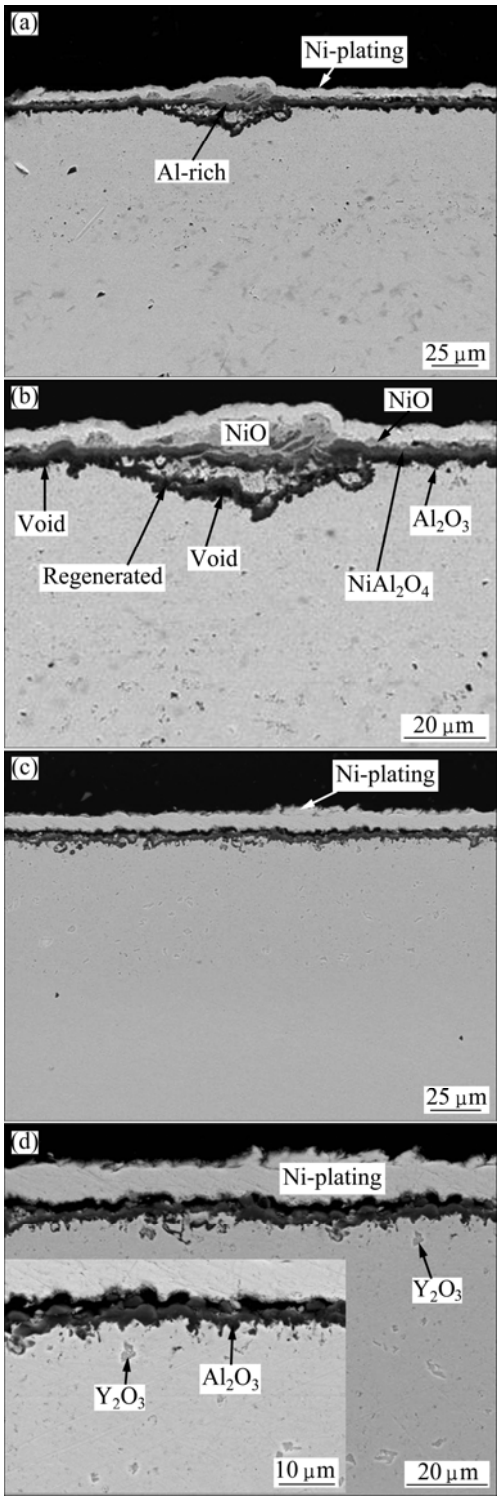

Fig. 8 Cross-sectional BSE images of oxide scales formed on pure Ni_3Al (a, b) and Y_2O_3-dispersed Ni_3Al (c, d) coating after cyclic oxidation in air at 900 °C for 100 h

magnification image shown in Fig. 8(d), NiO (bright color) and $NiAl_2O_4$ spinel (darker than NiO but lighter than Al_2O_3 in color contrast) are not observed. This implies that the time for the formation of the continuous alumina layer is shortened, in other words, the scale formed on the Y_2O_3-dispersed γ'-Ni_3Al coating is

composed mainly of alumina, which is also consistent well with XRD analysis. The alumina scale formed was further investigated using TEM, as seen in Fig. 9. It reveals that the grain size of the alumina formed on the Y_2O_3-free γ'-Ni_3Al coating is about 90 nm (Fig. 9(a)), while the alumina formed on the Y_2O_3-dispersed γ'-Ni_3Al coating is about 45 nm (Fig. 9(b)). Here, it is worthy to point out that interface cavities did not occur. From the comparison of Fig. 3 and Fig. 8, it can be found that voids in the coatings disappeared after 100 h oxidation due to the interdiffudion between the coatings and base metals.

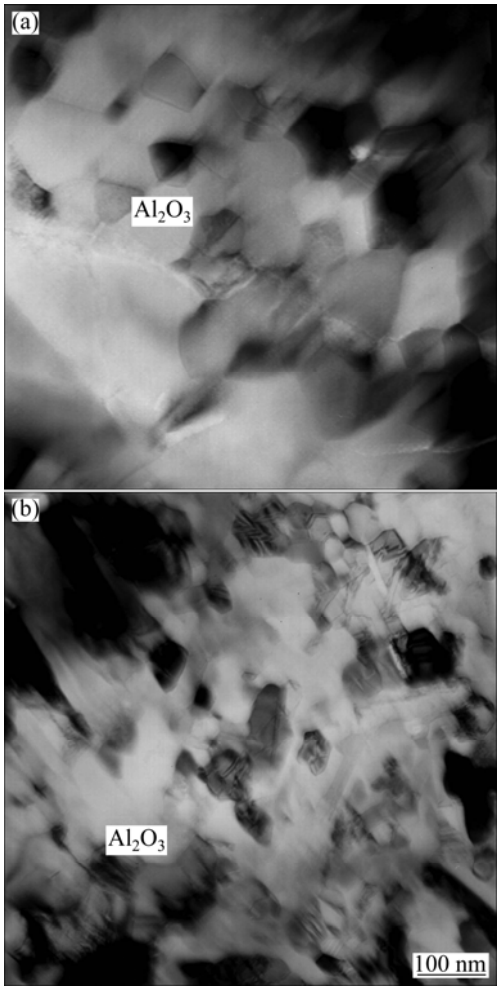

Fig. 9 TEM bright-field image of alumina scale formed on pure Ni_3Al (a) and Y_2O_3-dispersed Ni_3Al (b) coatings after cyclic oxidation in air at 900 °C for 100 h

4 Discussion

Scale failure on pure alumina-forming alloys and coatings during high temperature oxidation has been extensively studied [1−4, 6−15]. It is generally believed that the failure of oxide scale is related to internal compressive stresses resulting from the growth stress, the thermal stress, and the interfacial stress [20]. The formation of large interface cavities greatly decreases the critical stress (δ_c) for scale decohesion as expressed in the following equation [21]: $\delta_c=K_{IC}/(\pi c)^{1/2}$, where K_{IC} is the critical stress intensity factor and c is a half length of the interface defect. Generally speaking, the interface cavities form as a result of a condensation of excessive vacancies at the grain boundaries and/or the scale/coating interface. The vacancy flux may be induced either by dominant outward diffusion of Al cations through the scale, or by faster inward diffusion of Ni in the Al-depleted matrix adjacent to the scale due to a selective oxidation of Al. The existence of voids can significantly reduce the value of K_{IC} of the oxide scale. According to the equation, a large size of voids (c) and a low K_{IC} value give a very low critical stress (δ_c) for scale spallation. The high thermal stress during cooling as well as other residual stresses could induce scale cracking or de-cohesion around these voids, as shown in Fig. 6(a) and Fig. 8(b). The scale cracking or de-cohesion exposes the underlying coating directly to the air during the subsequent cyclic oxidation. Consequently, NiO nodules form on the fresh surface (Fig. 6(b) and Fig. 8(b)) because the aluminum content beneath the scale is too low and it cannot be compensated by the fast supply of aluminum from the coating due to the coarsening of the Ni_3Al grains. The growth of NiO progressively decreases the partial pressure of oxygen and simultaneously increases the Al content at the oxidation front, which leads to the selective oxidation of Al to form a regenerated alumina layer (Fig. 8(b)). Afterward, the NiO growth is completely prevented, leading to the improvement of the oxidation resistance. However, the regrowth of Al_2O_3 scale, as well as the inward diffusion of Al to the substrate, results in a rapid decrease of Al level in the coating matrix, deteriorates the coating performances and limits the lifetime of coating.

In contrast, no spallation and interface voids occurr on the Y_2O_3-dispersed γ'-Ni_3Al coating. On the basis, it is assumed that the addition of Y_2O_3 particles evidently enhances the adherence of the scale to the matrix and increases the threshold value of the scale for cracking or spalling. The so-called “reactive element effect” has been extensively studied [9−15]. The possible beneficial effects of Y_2O_3 during annealing and oxidation found in this investigation are summarized as follows.

First, adding Y_2O_3 into the electrodeposited Ni−Al composite coating further refines the grains of γ'-Ni_3Al coating [16,17], which significantly increases the number of sites for aluminia nucleating from the onset of oxidation, leading to the development of fine-grained alumina scale, as seen in Fig. 9. The fine-grained scale would be more adherent, because of easier operation of plastic deformation of the oxide in the thermal cycling [1]. At the same time, grain refining of γ'-Ni_3Al coating

may also help to develop a more adherent alumina scale by minimizing the formation of interface voids during thermal cycling [1,11,12].

Second, Y_2O_3 particles alter the growth mechanism and the morphology of Al_2O_3 scale. Some investigators [11,22] reported that the reactive element oxides such as CeO_2, La_2O_3,Y_2O_3 dispersed in alloys during oxidation would release a small amount of RE ions, some of which could enter into the growing alumina scale via the scale/grain boundaries. Finally, they reach the gas/scale interface. Due to a much lower diffusivity of RE ions along the scale/grain boundaries than that of Al cations, the outward diffusion of Al cations will be suppressed and the slow inward diffusion of oxygen will become dominant. Indirect evidence for the suppression of the dominant outward growth of alumina is shown in Fig. 7. The alumina scale consists of columnar grain crystals [22,23]; whereas the alumina scale whose growth is controlled by the outward diffusion of aluminium should exhibit a typical equiaxed grain structures [7]. The inward scale growth decreases the scaling rate (Fig. 5) and reduces the interface voiding kinetics (Fig. 8(d)). Furthermore, the RE oxide precipitates will be formed if a critical doping concentration of RE ions along the grain boundary is exceeded. Due to the solute-drag effect by RE ions or the precipitates, the scale/grain boundaries would be pinned [24], and fine-grained scales with enhanced adhesion could be retained.

Third, the Y_2O_3 particles themselves in the coating might act as sinks like CeO_2 particles for vacancy condensation[7,11,19], which decreases the number and size of vacancies at the scale/coating interface or in the coating, as seen in Fig. 8(d).

Fourth, the Y ions segregated to the interface scavenge the interface segregants of sulfur, a detrimental element which can promote the growth of the exiting interface voids or weaken the interface bonding [9]. Although the current research did not detect any sulphur at the scale/coating interface, but desulfidation treatment could significantly improve the adhesion of alumina scale [25].

5 Conclusions

1) An ultrafine-grained Y_2O_3-dispersed Ni_3Al coating was fabricated by annealing the as-deposited Ni−Al−Y_2O_3 composite at 800 °C for 3 h.

2) The coarse-grained Ni_3Al coating had a poor cyclic oxidation resistance at 900 °C, because the formation of large voids at the scale/metal interface caused buckling, cracking and spalling of the scale formed. In contrast, the ultrafine-grained Y_2O_3-dispersed Ni_3Al coating exhibited an excellent oxidation resistance.

3) The Y_2O_3 dispersions not only significantly refined the grain structure of the produced Ni_3Al coatings but also took REEs on its oxidation, which prevented the formation of interface cavity and consequently allowed the coating to intrinsically grow finer-grained adherent alumina scale.

References

[1] WANG F H. The effect of nanocrystallization on the selective oxidation and adhesion of Al_2O_3 scales [J]. Oxid Met, 1997, 47: 247−258.

[2] LA P Q, BAI M W, XUE Q J, LIU W M. A study of Ni_3Al on carbon steel surface via the SHS casting route [J]. Surface and Coatings Technology, 1999, 113: 44−51.

[3] SUSAN D F, MARDER A R. Oxidation of Ni−Al-based electrodeposited composite coatings (II): Oxidation kinetics and morphology at 1000 °C [J]. Oxid Met, 2002, 57: 159−180.

[4] LIU H F, CHEN W X. Porosity-dependent cyclic-oxidation resistance at 850 °C of annealed Ni−Al-based coatings via electroplating [J]. Surface and Coatings Technology, 2008, 202: 4019−4027.

[5] YANG X, PENG X, WANG F. Size effect of Al particles on the structure and oxidation of Ni/Ni_3Al composites transformed from electrodeposited Ni−Al films [J]. Scripta Materialia, 2007, 56: 509−512.

[6] LIU H F, CHEN W X. Cyclic oxidation behavior of electrodeposited Ni_3Al-CeO_2 base coatings at 850 °C [J]. Oxid Met, 2005, 64: 331−354.

[7] LIU H F, CHEN W X. Cyclic oxidation behaviour of electrodeposited Ni_3Al−CeO_2 base coatings at 1050 °C [J]. Corrosion Science, 2007, 49: 3453−3478.

[8] CHOI S C, CHO H J, KIM Y J, LEE D B. High-temperature oxidation behavior of pure Ni_3Al [J]. Oxid Met, 1996, 46: 51−72.

[9] LEES D G. On the reasons for the effects of dispersions of stable oxides and additions of reactive elements on the adhesion and growth-mechanisms of chromia and alumina scales-the “sulfur effect” [J]. Oxid Met, 1987, 27: 75−81.

[10] BRUMM M W, GRABKE H J. Oxidation behaviour of NiAl-(II): Cavity formation beneath the oxide scale on NiAl of different stoichiometries [J]. Corrosion Science, 1993, 34: 547−561.

[11] XU C, PENG X, WANG F. Cyclic oxidation of an ultrafine-grained and CeO_2-dispersed δ-Ni_2Al_3 coating [J]. Corrosion Science, 2010, 52: 740−747.

[12] PENG X, LI M, WANG F. A novel ultrafine-grained Ni_3Al with incresaed cyclic oxidation resistance [J]. Corrosion Science, 2011, 53: 1616−1620.

[13] RAHMEL A, SCHUTZE M. Mechanical aspects of the rare-earth effec [J]. Oxid Met, 1992, 38: 255−266.

[14] JUNG H G, KIM KY. Effect of yttrium coating on the oxidation behavior of Ni_3Al [J]. Oxid Met, 1996, 46: 147−167.

[15] PINT B A. The oxidation behavior of oxide-dispersed β-NiAl: (I). short-term performance at 1200 °C [J]. Oxid Met, 1998, 49: 531−559.

[16] ZHOU Y B, ZHANG H J, WANG Z T. Effect of Y_2O_3 on the microstructure and oxidation of γ-Ni+γ'-Ni_3Al coatings transformed from electrodeposited Ni−Al films at 1000 °C [J]. Transactions of Nonferrous Metals Society of China, 2008, 18(2): 297−302.

[17] ZHOU Y B, ZHAO G G, ZHANG H J, ZHANG Y C, QIAN B Y. Effect of CeO_2 on the microstructure and isothermal oxidation of Ni−Al alloy coatings transformed from electrodeposited Ni−Al films at 800 °C [J]. Vacuum, 2009, 83: 1333−1339.

[18] ZHOU Y B, QIAN B Y, ZHANG H J. Al particles size effect on the microstructure of the co-deposited Ni−Al composite coatings [J]. Thin Solid Films, 2009, 517: 3287−3291

[19] ZHOU Y, PENG X, WANG F. Cyclic oxidation of alumina-forming Ni−Al nanocomposites with and without CeO_2 addition [J]. Scripta Materialia, 2006, 55: 1039−1042.

[20] BULL S J. Modeling of residual stress in oxide scales [J]. Oxid Met, 1998, 49: 1−17.

[21] HANCOCK P, NICHOLLS J R. Application of fracture mechanics to failure of surface oxide scales [J]. Mater Sci Technol, 1988, 4: 398−406.

[22] STOTT F H, WOOD G C, STRINGER J. The influence of alloying elements on the development and maintenance of protective scales [J]. Oxid Met, 1995, 44: 113−141.

[23] PRESCOTT R, GRAHAM M J. The formation of aluminum oxide scales on high-temperature alloys [J]. Oxid Met, 1992, 38: 233−254.

[24] HINDAM H M, WHITTLE D P. Peg formation by short-circuit diffusion in Al_2O_3 scales containing oxide dispersions [J]. J Electrochem Soc, 1982, 129: 1147−1149.

[25] GRABKE H J. Oxidation of NiAl and FeA [J]. Intermetallics, 1999, 7: 1153−1158.

Y_2O_3 改性细晶 Ni_3Al 合金涂层在 900 °C 下的循环氧化性能

周月波，张海军

黑龙江科技学院 材料科学与工程学院，哈尔滨 150027

摘　要：将 Ni−Al 和 Ni−Al/Y_2O_3 复合镀层分别在 800 °C 下扩散 3 h 制备纯 Ni_3Al 和 Y_2O_3 改性的 Ni_3Al 合金涂层，对其显微组织和氧化性能进行对比研究。SEM/EDAX 和 TEM 分析表明，涂层中 Y_2O_3 的加入抑制了合金化过程中基体晶粒的长大。在 900 °C 下循环氧化 100 h 的结果表明，Y_2O_3 的加入明显提高了 Ni_3Al 合金涂层的抗循环氧化性能。对 Y_2O_3 影响 Ni_3Al 涂层的结构和氧化性能的机理进行了分析。

关键词：电镀；Ni_3Al；循环氧化；活性元素效应

(Edited by YUAN Sai-qian)